

# A Potentiometric Electronic Skin for Thermosensation and Mechanosensation

Xiaodong Wu, Juan Zhu, James W. Evans, Canhui Lu, and Ana C. Arias\*

Electronic skins (e-skins) that mimic the thermosensation and mechanosensation functionalities of natural skin are highly desired for the emerging fields of prosthetics and robotics. Advances in the materials and architecture of e-skins have been made; nevertheless, sensing mechanism innovations are rarely explored. Here, inspired by the skin sensory behaviors, a single potentiometric sensing scheme for both thermosensation and mechanosensation functionalities are presented. Through careful materials selection, component optimization, and structure configuration, the coupling effect between thermosensation and mechanosensation can be significantly minimized. Such a potentiometric sensing scheme enables one to create a new class of energy-efficient e-skin with distinctive characteristics that are highly analogous to those of natural human skin. The e-skin reported here features ultralow power consumption (at nanowatt level), greatly simplified operation (only voltage output), ultrahigh sensitivity (non-contact sensing capability), all-solution-processing fabrication, and, more importantly, good capability for simultaneous monitoring/mapping of both thermal and mechanical stimulations. In addition to proposing a new sensory mechanism, integration of the dual-functional e-skin with a soft robotic gripper for object manipulation is demonstrated. The presented concise yet efficient sensing scheme for both thermosensation and mechanosensation opens up previously unexplored avenues for the future design of skin prosthetics, humanoid robotics, and wearable electronics.

(in the temperature range of 5–48 °C),<sup>[2,3]</sup> while mechanoreceptors (including slow-adapting receptors and fast-adapting receptors) respond to innocuous mechanical stimuli (e.g., pressure, touch, and vibration).<sup>[4,5]</sup> These two essential sensory functions provide valuable information about the surroundings and also enable us to protect our body tissues from damages.<sup>[6]</sup> To mimic these two functionalities, individual thermal sensors (based on thermoresistive, p–n junctions, thermoelectric, and pyroelectric mechanisms)<sup>[1,7–9]</sup> and mechanical sensors (based on resistive, capacitive, optical, transistor-based, triboelectric, and piezoelectric mechanisms)<sup>[10–12]</sup> have been developed and establish the foundations for the burgeoning fields of wearable electronics, human–machine interfaces, and the Internet of Things. Nevertheless, achieving both thermosensation and mechanosensation functionalities in a single and simple system still remain challenging.

In recent years, artificial electronic skins (e-skins) have been actively explored by integrating thermal sensing elements and mechanical sensing elements.<sup>[13–22]</sup>

## 1. Introduction

Thermosensation and mechanosensation are two primary functions of the human skin, allowing us to interact with the world efficiently.<sup>[1]</sup> Within the human skin, thermoreceptors (including cold receptors and warm receptors) respond to thermal stimuli

For example, flexible networks of thermal and mechanical sensors were fabricated via combining temperature and pressure sensing elements with organic transistor active matrixes.<sup>[13]</sup> A flexible bimodal sensor array for simultaneous detection of temperature and pressure was also developed based on specially designed field-effect transistors with piezo-pyroelectric gate dielectric and piezo-thermoresistive semiconductor channel.<sup>[14]</sup> Additionally, an optical sensor system with Fabry–Perot interferometers and photonic crystal structures for both temperature and pressure monitoring was demonstrated recently.<sup>[15]</sup> Nevertheless, these sensing devices involve sophisticated architectures and demand nontrivial fabrication procedures, posing a challenge for their large-scale applications. To simplify the architecture and fabrication of e-skins, multimode sensors that can detect both thermal and mechanical stimuli are developed. For instance, structurally engineered conductive thermoelectric materials<sup>[16]</sup> as well as pyroelectric materials<sup>[17]</sup> are employed to fabricate multimode sensors for temperature and pressure detection. Despite these pioneering achievements, most of the existing e-skins suffer from mutual interference/crosstalk between thermotransduction and mechanotransduction, which is difficult to eliminate. In addition, the majority of

Dr. X. Wu, Dr. J. Zhu, Prof. A. C. Arias  
Department of Electrical Engineering and Computer Sciences  
University of California  
Berkeley, CA 94720, USA  
E-mail: acarias@eecs.berkeley.edu

Prof. J. W. Evans  
Department of Materials Science and Engineering  
University of California  
Berkeley, CA 94720, USA

Prof. C. Lu  
State Key Laboratory of Polymer Materials Engineering  
Polymer Research Institute of Sichuan University  
Chengdu 610065, China

 The ORCID identification number(s) for the author(s) of this article can be found under <https://doi.org/10.1002/adfm.202010824>.

DOI: 10.1002/adfm.202010824

these e-skins rely on a continuous external power supply, and the power consumption could reach as high as tens of mW per single device,<sup>[23]</sup> which hinders their large-scale deployment and long-term operation. Moreover, the mismatch and incompatibility of signal outputs from different sensing modules increase the complexity of the measurement setups and further elevate the power consumption. Therefore, simplifying the fabrication and operation of e-skins, reducing the power consumption, and minimizing the coupling effect between thermotransduction and mechanotransduction present fundamental challenges for the future versions of e-skins.

Motivated by the limitations of the existing e-skins, here, we realize both thermosensation and mechanosensation functionalities via a single potentiometric sensing scheme, which is based on thermally- or mechanically-regulated variations in potential difference measured between two active electrodes. Through careful materials selection, component tuning, and structural engineering of sensor systems, we can significantly minimize the coupling effect between the thermosensation and mechanosensation processes, realizing continuous monitoring of both thermal and mechanical stimuli. In addition, the potentiometric e-skin presented here does not rely on external power supply, featuring an ultralow power consumption (at nanowatt level). We also demonstrate the capability of this e-skin for temperature and pressure monitoring and mapping simultaneously. Experiment results show that the proposed thermal and mechanical sensing devices exhibit ultrahigh sensitivity, which enables to thermally detect a warm object in a non-contact sensing style and allows us to mechanically detect airflow continuously. The thermal sensing range (5–50 °C) and mechanical sensing range (kilopascal to megapascal) are highly analogous to that of natural human skin.<sup>[1–3]</sup> Moreover, we use an all-solution-processing approach in the fabrication of the e-skin, which leads itself to possess scalability and cost-efficiency. To the best of our knowledge, this is the first demonstration of an artificial e-skin with remarkable energy-efficiency, high performance combined functionalities in one system, and highly analogous response behavior to that of natural skin (see Table S1 and Note S1, Supporting Information, for comparison with the state-of-the-art e-skins). This concise, multifunctional, and high-performance sensing scheme provides a new design philosophy for future skin prosthetics, humanoid robotics, bioelectronics, and wearable healthcare devices.

## 2. Results and Discussion

### 2.1. Design Concept of the Potentiometric Electronic-Skin

In natural skin sensory system (Figure 1a), the thermoreceptors and mechanoreceptors give us the means to perceive thermal and mechanical stimuli due to variations of membrane potential. Fundamentally, a potential difference is formed across the sensory cell membrane due to the asymmetric ion distribution.<sup>[24,25]</sup> When the sensory cells are subjected to a thermal or mechanical stimulus, the thermally gated or mechanically gated ion channels will be opened, with the ions flowing through the channels. This leads to a significant variation in the membrane potential of the sensory cells (i.e., receptor potential, Figure 1b).

The receptor potential is encoded into an action potential and then transmitted to the brain through the axon to form sensory feedback.<sup>[1]</sup> This sensing principle makes the human skin a highly effective and low energy consumption sensory system.<sup>[26]</sup> To mimic the response behaviors of the skin sensory system, we design an artificial e-skin for both thermosensation and mechanosensation based on a single potentiometric sensing mechanism, as illustrated in Figure 1c. This e-skin is composed of arrays of potentiometric thermal sensors and potentiometric mechanical sensors. The operating principle of these potentiometric sensors is based on thermally- or mechanically-regulated variations in potential difference measured between two active electrodes. The response behaviors of the potentiometric thermal sensors and mechanical sensors are highly analogous to those of natural skin sensory receptors (Figure 1d). Specifically, a variation in sensor potential could be triggered by an externally applied thermal or mechanical stimulus, as demonstrated in Movies S1 and S2, Supporting Information, where temperature and pressure variations caused by a finger touch could be well perceived. Remarkably, our thermal sensors exhibit ultrahigh sensitivity and can even perceive the approach of a warm object (e.g., human hand) in a non-contact sensing style (Movie S3, Supporting Information). Such bioinspired thermosensation and mechanosensation functionalities enable us to interact effectively with the surroundings in an energy-efficient way.

### 2.2. Operating Mechanism of Potentiometric Thermosensation and Mechanosensation

The potentiometric thermosensation and mechanosensation operating mechanism is described in Figure 2. When two active electrode materials are brought into contact with an appropriate electrolyte, a potential difference is developed between the two electrodes due to the different oxidation–reduction equilibrium reactions at the electrode/electrolyte interfaces.<sup>[27]</sup> We employ Prussian blue-modified graphite carbon (PB/carbon) and silver/silver chloride (Ag/AgCl) as the two active electrodes and use polyvinyl alcohol/sodium chloride/glycerol (PVA/NaCl/Gly) ionic composites as the electrolyte. A potential difference can be recorded between the PB/carbon and Ag/AgCl electrodes when they are in contact with the PVA/NaCl/Gly electrolyte (Figure 2a, see Figure S1, Supporting Information, for more discussion). Notably, the measured potential difference output is closely related to the internal impedance between the two electrodes. As depicted in Figure 2b, when the internal impedance is very low (e.g.,  $< \approx 1 \text{ M}\Omega$ ), the potential difference is fully released, and the device is in an “On” state. In contrast, when the internal impedance is very high (e.g.,  $> \approx 100 \text{ M}\Omega$ ), the potential difference output is practically cut off and the device is in an “Off” state. When the internal impedance ranges between  $\approx 1$  and  $\approx 100 \text{ M}\Omega$ , the measured potential difference output shows a strong dependence on the internal impedance, exhibiting a “Transition” phase. We record and characterize this “Transition” process in order to encode thermal or mechanical stimuli into the variations of the potential difference output measured between the two electrodes, reflecting the potentiometric thermosensation or mechanosensation working principle.

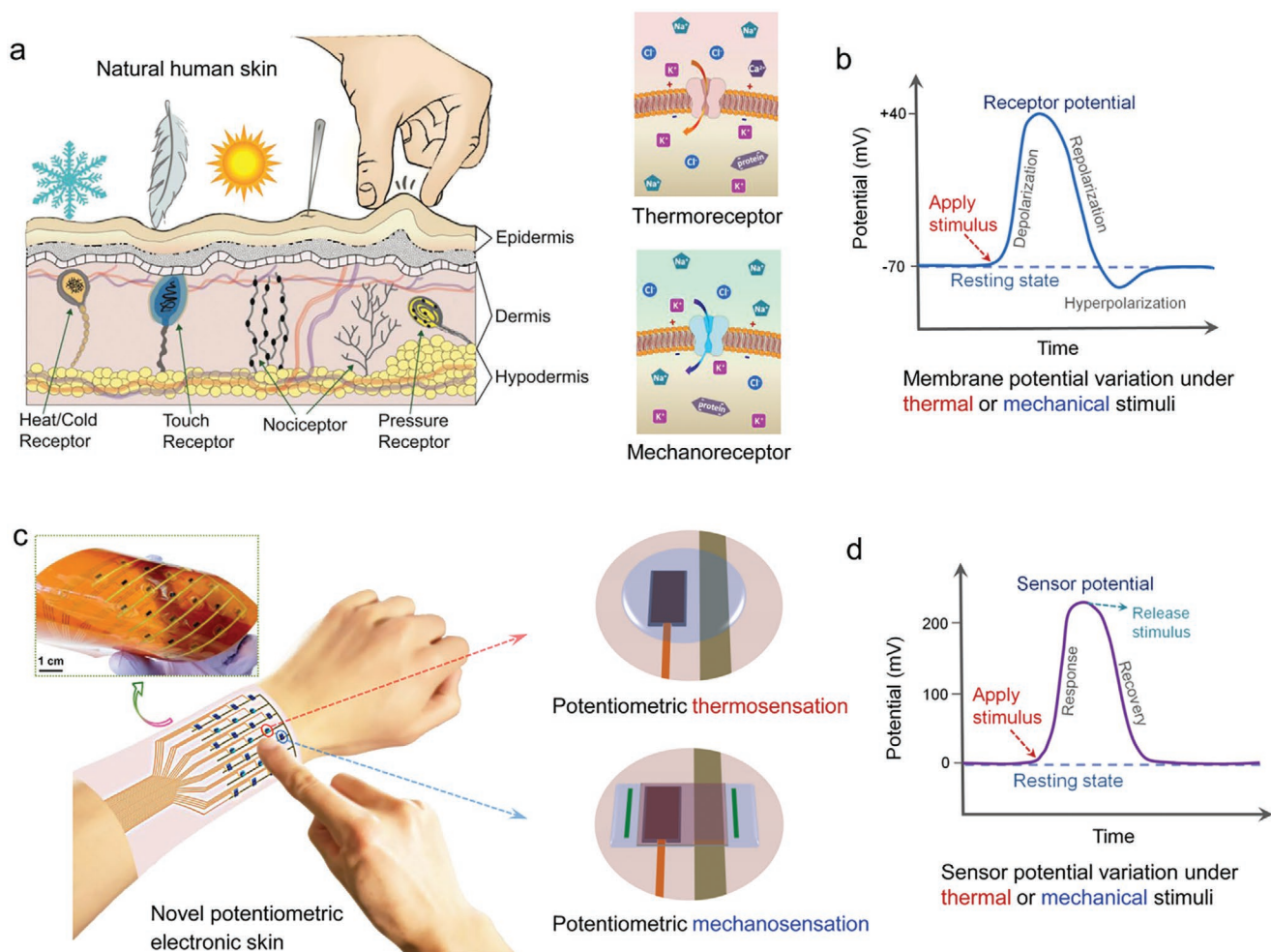


**Figure 1.** Bioinspired design of potentiometric e-skin for both thermosensation and mechanosensation. a) Illustrations depicting the thermoreceptors and mechanoreceptors in natural skin sensory system.<sup>[24,25]</sup> b) Schematic showing the response behaviors of natural thermoreceptors and mechanoreceptors to external stimuli based on the variation in membrane potential. c) Photograph and schematics showing an artificial e-skin based on a single potentiometric sensing scheme for both thermosensation and mechanosensation. d) Schematic illustrating the response behaviors of the potentiometric thermal sensors and mechanical sensors to external stimuli based on the variation in sensor potential.

The potentiometric thermosensation principle is based on temperature-regulated intrinsic impedance variation of the PVA/NaCl/Gly electrolyte (Figure 2c), as an increase in temperature results in an increase in the ionic conductivity and a decrease in the impedance of electrolyte.<sup>[28–31]</sup> As verified in Figure 2e, the intrinsic impedance of PVA/NaCl/Gly-2% electrolyte (PVA/NaCl/Gly-*X*% signifies the weight ratio of Gly:PVA is *X*%) decreases prominently when varying the temperature from 5 to 50 °C. Similarly, the measured potential difference output of the devices changes significantly with temperature, resulting in a potentiometric thermosensation response. The potentiometric mechanosensation process is based on mechanically regulated interfacial impedance variation of the electrode/electrolyte interfaces (Figure 2d). Via creating a periodic microstructure on the electrolyte surface, the electrode/electrolyte interfaces can be modulated continuously and efficiently by an externally applied force. As shown in Figure 2g, applying mechanical stimuli on the devices can greatly reduce the electrode/electrolyte interfacial impedance. The measured potential

difference output of the devices shows a significant increase with the applied force, resulting in a potentiometric mechanosensation process.

The coupling effect between the thermosensation and mechanosensation processes can be significantly minimized via rational component optimization of the electrolyte system. The intrinsic impedance and electrochemical property of the PVA/NaCl/Gly electrolyte can be optionally manipulated by tuning the concentration of Gly, which acts as a humectant for modulating the water content in the electrolyte (see Figures S2 and S3, Supporting Information, for detailed discussion). Incorporating more Gly into the electrolyte can efficiently increase the water content and reduce the intrinsic impedance of the electrolyte. For the potentiometric thermosensation, we employ PVA/NaCl/Gly electrolyte with relatively low Gly content (e.g., PVA/NaCl/Gly-2%) and high impedance. The intrinsic impedance of PVA/NaCl/Gly-2% is located in the “Transition” range (in Figure 2b) and can be directly used for thermosensation (Figure 2e). In contrast, for the potentiometric mechanosensation, we choose

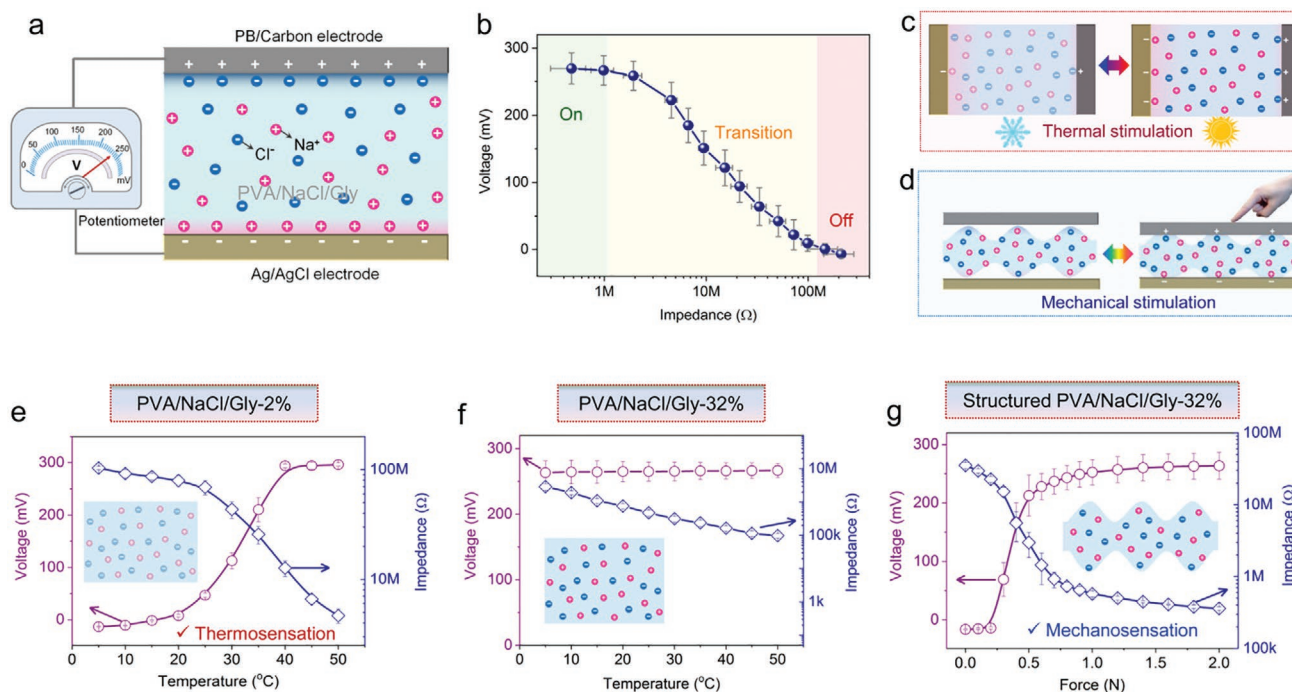


**Figure 2.** Operating mechanism of potentiometric thermosensation and mechanosensation. a) Schematic showing the creation of a potential difference between PB/carbon and Ag/AgCl electrodes with a PVA/NaCl/Gly electrolyte. b) Correlation between the measured potential difference output and the internal impedance between the two electrodes. c,d) Working principles of potentiometric thermosensation via thermal regulation of the intrinsic impedance of the electrolyte (c) and potentiometric mechanosensation via mechanical regulation of the electrode/electrolyte interfacial impedance (d). e,f) Variation in the internal impedance and voltage output measured between the two electrodes under different temperatures when using PVA/NaCl/Gly-2% (e) and PVA/NaCl/Gly-32% (f) as the electrolyte. g) Variation in the internal impedance and voltage output measured between the two electrodes under different applied forces when using microstructured PVA/NaCl/Gly-32% as the electrolyte.

PVA/NaCl/Gly electrolyte with relatively high Gly content (e.g., PVA/NaCl/Gly-32%) and low impedance. The intrinsic impedance of PVA/NaCl/Gly-32% also varies with temperature, but the variation is limited within the “On” range (in Figure 2b). As a result, the measured potential difference output of PVA/NaCl/Gly-32% devices keeps stable despite the temperature variation, as confirmed in Figure 2f. Such temperature-insensitive signal output of PVA/NaCl/Gly-32% devices is not favorable for thermosensation but is highly desired for an autonomous mechanosensation process. We utilize another strategy, creating microstructure on the PVA/NaCl/Gly-32% electrolyte surface, to efficiently regulate the electrode/electrolyte interfacial impedance, realizing a potentiometric mechanosensation process (Figure 2g). Hence, we can achieve both thermosensation and mechanosensation simultaneously via rational manipulation of the electrolyte.

### 2.3. Potentiometric Thermal Sensors and Mechanical Sensors

The configuration and photograph of the potentiometric thermal sensors are shown in Figure 3a–c. Their fabrication via an all-solution-processing approach is illustrated in Figure S4, Supporting Information. Temperature variations can change the ionic conductivity and intrinsic impedance of the PVA/NaCl/Gly electrolyte significantly. When the temperature rises, the intrinsic impedance of the PVA/NaCl/Gly electrolyte

shows a prominent decline (Figure 3d) and the measured voltage output between the two electrodes increases with temperature (Figure 3e). It is noticed that the thermal sensors have an optimum operation range, within which temperature can be monitored continuously. As an example, for thermal sensors with PVA/NaCl/Gly-2% electrolyte, the operation range is around 10–40 °C, which is very close to the sensing range of natural skin thermoreceptors.<sup>[1–3]</sup> The response behaviors of the thermal sensors can be effectively regulated via tuning the Gly content in the electrolyte. For example, in the temperature range of 20–30 °C, the sensitivity of sensors with PVA/NaCl/Gly-4% electrolyte ( $\approx 14.9 \text{ mV } ^\circ\text{C}^{-1}$ ) is much higher than that of sensors with PVA/NaCl/Gly-0.5% electrolyte ( $\approx 5.2 \text{ mV } ^\circ\text{C}^{-1}$ ). Also, sensors with electrolyte of higher Gly content exhibit a lower detection range and vice versa (Figure 3d–e), revealing good tunability of the thermal sensors.

The configuration of the potentiometric mechanical sensors is shown in Figure 3f. Applying a force on the devices can increase the contact area of the electrode/electrolyte interfaces, giving rise to a variation in the potential difference output measured between the two electrodes. The mechanical sensors, as illustrated and shown in Figure 3g,h, are also fabricated via an all-solution-processing process (Figure S5, Supporting Information), revealing good scalability and cost-efficiency. Uniform and periodic microstructure, which enables to regulate the electrode/electrolyte interfaces smoothly and continuously, is created on the PVA/NaCl/Gly electrolyte surface via a scalable

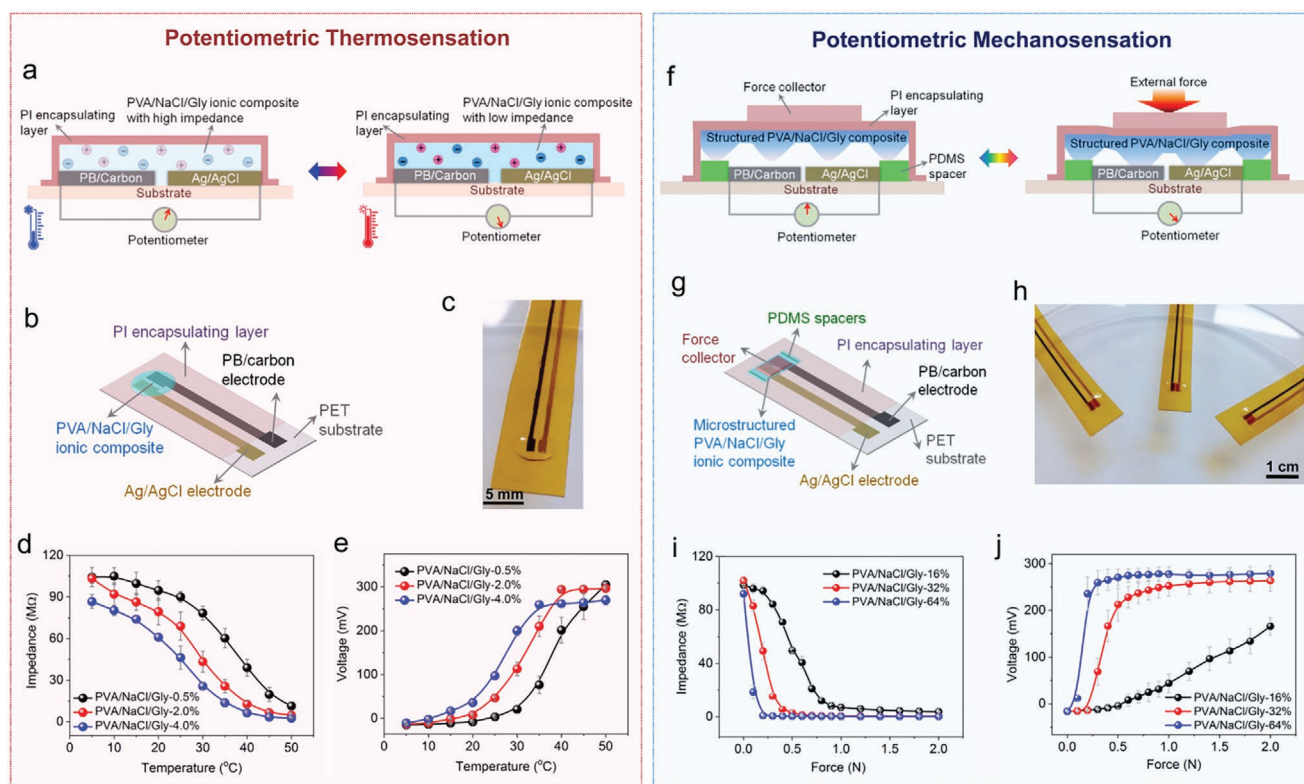


**Figure 3.** Potentiometric thermal sensors and mechanical sensors. a) Working principle of the potentiometric thermal sensors based on temperature-regulated intrinsic impedance change of the ionic composite electrolyte. b, c) Configuration and photograph of a potentiometric thermal sensor. d, e) Impedance variation of the PVA/NaCl/Gly electrolytes with different Gly contents (d) and signal outputs of the corresponding thermal sensors (e) under different temperatures. PVA/NaCl/Gly-X% signifies the weight ratio of Gly:PVA is X%. f) Schematic illustrations showing the cross section of the mechanical sensors before and after applying a force on the devices. g, h) Configuration and photograph of the potentiometric mechanical sensors. i, j) Impedance variation measured between the two electrodes when using microstructured PVA/NaCl/Gly ionic composites of different Gly contents as the electrolyte (i) and signal outputs of the corresponding mechanical sensors (j) under different applied forces. The contact area of the applied force is  $\approx 15 \text{ mm}^2$ .

mesh-molding method (Figure S6, Supporting Information). The impedance measured between the two electrodes can be efficiently regulated by an externally applied force, as verified in Figure 3i. As a result, the measured voltage output of the sensors varies significantly with the applied force (Figure 3j). Notably, the response behaviors of the mechanical sensors are highly tunable through modulating the Gly content in the PVA/NaCl/Gly electrolyte. Sensors with electrolyte of higher Gly content show lower detection limit and higher sensitivity, while sensors with electrolyte of lower Gly content exhibit broader detection range, exhibiting good tunability of the mechanical sensors. For instance, in the force range of 0–1 N, the sensitivity of sensors with PVA/NaCl/Gly-64% electrolyte ( $\approx 278 \text{ mV N}^{-1}$ ) is much higher than that of sensors with PVA/NaCl/Gly-16% electrolyte ( $\approx 44 \text{ mV N}^{-1}$ )

#### 2.4. Performance of Thermosensation and Mechanosensation

The response behaviors of the potentiometric thermal sensors were investigated in water baths of controlled temperature. When the sensors at room temperature were immersed into a warm water bath of  $35 \text{ }^{\circ}\text{C}$ , the signal output of the devices

increased gradually and reached a steady state after a while (Figure 4a). With the sensors removed from the warm water, the signal output recovered to the initial value gradually. In contrast, when the sensors were immersed into a cold water bath of  $15 \text{ }^{\circ}\text{C}$ , the signal output of the devices decreased gradually (Figure 4b). After removing the sensors from the cold water bath, the signal output went back to the beginning state. Notably, when the thermal sensors were subjected to repeated temperature variations, as shown in Figure 4c and Figure S7, Supporting Information, the voltage outputs exhibit good repeatability and reliability. The response time of the thermal sensors measured under the above conditions is  $7.8 \pm 2.8 \text{ s}$ . Also, the thermal sensors are highly sensitive and can perceive the temperature variation caused by a finger touch (Movie S1, Supporting Information), and can even perceive the approach of a warm object (e.g., human hand,  $31 \text{ }^{\circ}\text{C}$ ) in a non-contact sensing style, as demonstrated in Figure 4d and Movie S3, Supporting Information. These results show that both static and dynamic temperature variations can be monitored continuously with these potentiometric thermal sensors. More importantly, the voltage output of the sensors is totally self-generated, eliminating the necessity of an external power supply. Thermoelectric and pyroelectric sensing devices

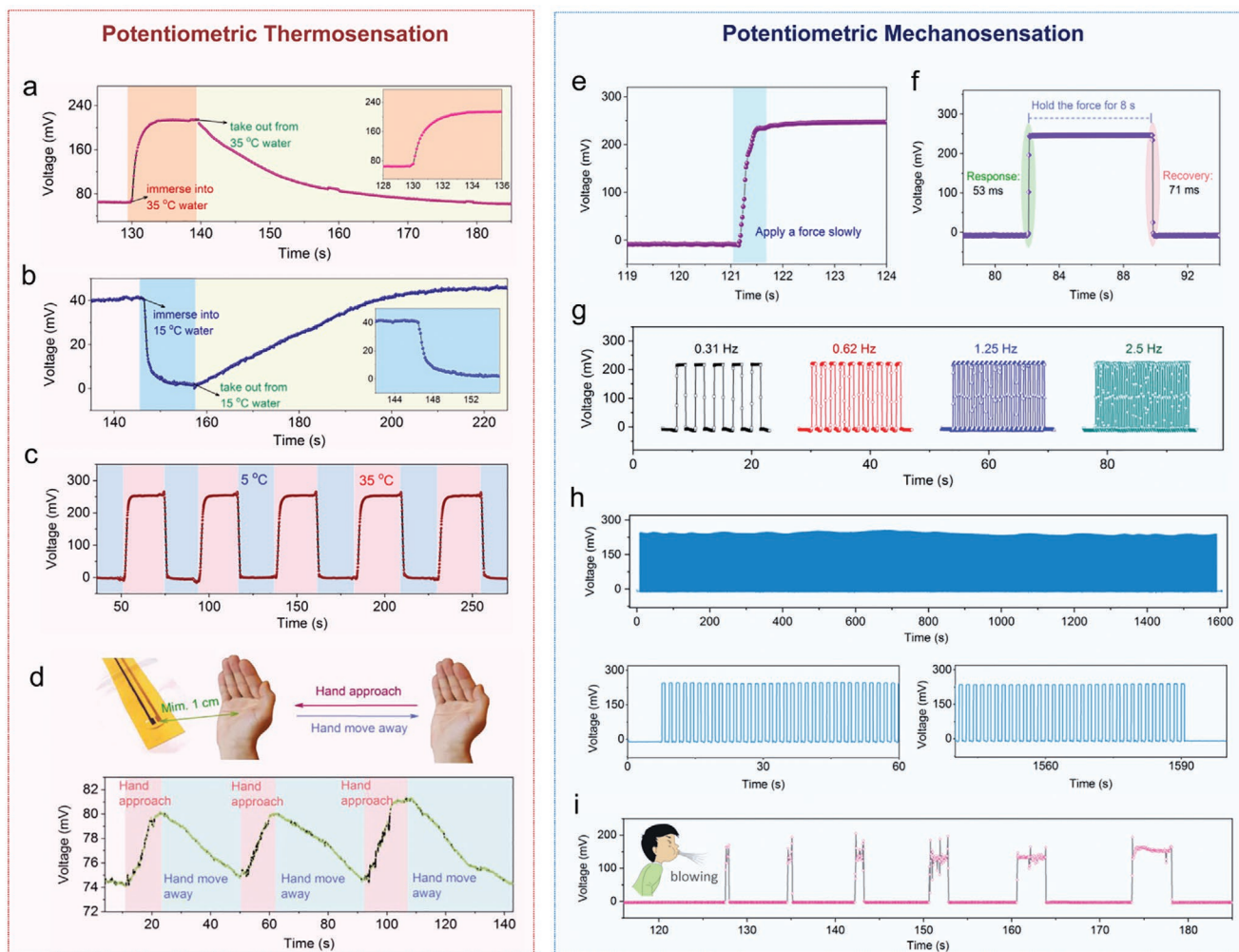


**Figure 4.** Potentiometric thermosensation performance and mechanosensation performance. a,b) Signal output of the thermal sensors (with PVA/NaCl/Gly-2% electrolyte, under 24 °C ambient temperature) when they are immersed into warm water bath of 35 °C (a) or cold water bath of 15 °C (b), followed by taking the sensors out from the water baths. c) Measured signal output of the thermal sensors when they are alternatively immersed into water baths of different temperatures. d) Non-contact thermosensation behavior of the thermal sensors to the approach of a warm hand ( $\approx 31$  °C) with the minimum distance of  $\approx 1$  cm. In the whole process, the warm hand does not directly touch or contact the thermal sensors, but the warm hand can still be perceived and detected, revealing the ultrahigh sensitivity of the thermal sensors. e) Response behavior of the mechanical sensors (with micro-structured PVA/NaCl/Gly-32% electrolyte) when gradually applying a force onto the devices. f) Response/recovery speed of the mechanical sensors measured by applying/releasing a static force to the devices. g) Signal outputs of the mechanical sensors when they are subjected to dynamic stimuli of different frequencies. h) Cyclic test of the mechanical sensors by loading–unloading a force to the devices for 1000 cycles. i) Response behavior of mechanical sensors to air blowing from the mouth, revealing high mechanosensation sensitivity of the sensors.

can also self-generate signal outputs under thermal stimuli, but they only respond to a temperature gradient or transient temperature variation, unable to monitor constant or slowly varying temperature.<sup>[9,16,17,32–34]</sup> This proposed potentiometric thermosensation mechanism provides a new methodology to compensate for this limitation.

The real-time response behaviors of the potentiometric mechanical sensors to a finger touch are presented in Movie S2, Supporting Information. When gradually applying a force onto the devices, the measured voltage output shows a smooth and continuous upswing (Figure 4e). When maintaining the applied force for a period of time, the signal output of the sensors remains highly stable, as shown in Figure 4f. The response and recovery time of the sensors is measured to be 53 and

71 ms, respectively (Figure 4f). These results verify the ability of the potentiometric sensors in monitoring slowly varying as well as static mechanical stimuli, which can compensate for the deficiency of piezoelectric and triboelectric sensing devices that selectively respond to dynamic mechanical stimulations.<sup>[1,35]</sup> These sensors are also capable of monitoring dynamic mechanical stimuli of adequate frequency (from 0.31 to 2.5 Hz), as demonstrated in Figure 4g. In addition, the mechanical sensors exhibit desirable durability and reliability during repeated loading–unloading of an external force onto the devices (Figure 4h). Moreover, ultrahigh sensitivity can be achieved by removing the PDMS spacers and replacing the polyimide encapsulation layer with a soft polyethylene film. Airflow generated by blowing from the mouth can be well detected and

monitored (Figure 4i). These results verify the good capability of the potentiometric mechanosensation devices in resolving diverse mechanical stimuli.

It is worth pointing out that the thermosensation process relies primarily on the temperature-regulated intrinsic impedance variation of the PVA/NaCl/Gly electrolyte, while the mechanosensation process depends mainly on the mechanically regulated electrode/electrolyte interfacial impedance variation. Via careful component regulation and structural engineering of the electrolyte, the interference between thermal sensing and mechanical sensing could be minimized as demonstrated in Figure S8, Supporting Information, and Figure 2e–g, thus to realize thermosensation and mechanosensation simultaneously. The stability of the proposed potentiometric sensors is fully discussed in Figure S9, Supporting Information. Compared with the state-of-the-art e-skins that can detect both thermal and mechanical stimulations (Table S1 and Note S1, Supporting Information), the potentiometric e-skin presented here exhibits several distinctive advantages, including unprecedented economic efficiency (i.e., using one material system to realize two autonomous functionalities), ultralow power consumption, simplified operation (i.e., only potentiometric measurement), ultrahigh sensitivity, and scalable fabrication.

## 2.5. Soft Robotic Gripper with Thermosensation and Mechanosensation Functions

Agile and dexterous object manipulation is an intriguing dream for robotic scientists, which, however, is confronted with a myriad of challenges.<sup>[36]</sup> Human hands are equipped with mechanoreceptors and thermoreceptors, and can effortlessly perform various manipulation tasks. For example, we can easily pick up a glass of water with our hands by applying the right amount of force. The glass does not slip from too small force, or break under too large force. Moreover, our fingers can perceive the temperature of the water (e.g., icy, warm, or hot). Although this is a routine operation in our daily life, it is a challenging set of tasks for a robotic hand. Here, we try to mimic these functionalities of human hands by the alliance of a soft robotic gripper and the proposed potentiometric thermal sensor as well as potentiometric mechanical sensor. As shown in Figure 5a,b, the soft robotic gripper comprises three components including an air inlet connector, a soft elastomeric body with pneumatic channels, and a strain-limiting layer (see Figure S10, Supporting Information, for the fabrication process), and can be pneumatically actuated and controlled. Potentiometric thermal sensors and mechanical sensors can be installed onto the fingers of the soft gripper to monitor the mechanical and thermal stimuli

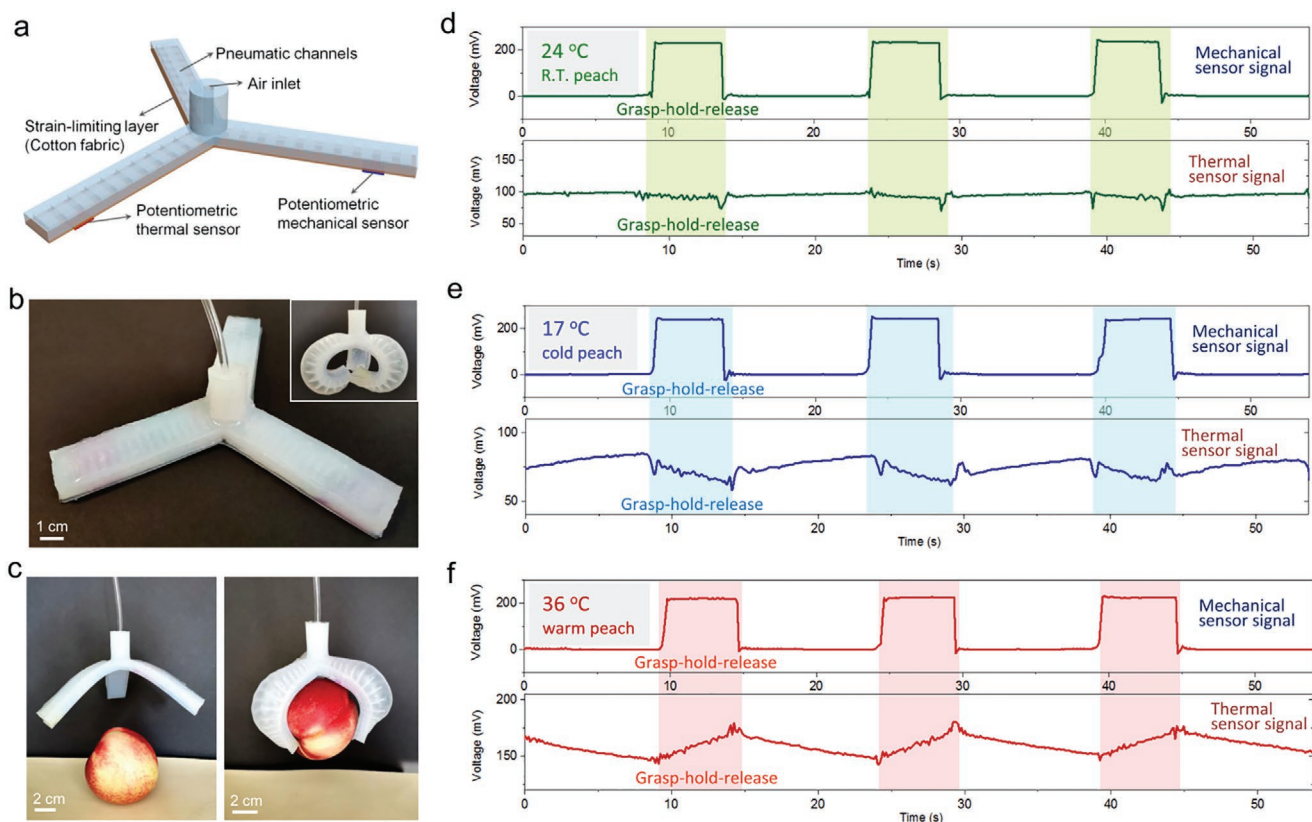


**Figure 5.** Soft robotic gripper with thermosensation and mechanosensation functionalities. a,b) Schematic and photograph showing a soft pneumatic gripper, onto which a potentiometric thermal sensor (PVA/NaCl/Gly-4%) and a potentiometric mechanical sensor (PVA/NaCl/Gly-32%) can be installed for the realization of both thermosensation and mechanosensation functionalities. c) Pictures showing the object (e.g., peach) manipulation with the soft pneumatic robotic gripper. d–f) Recorded signal outputs of the potentiometric thermal sensor and the potentiometric mechanical sensor when grasping–holding–releasing peaches of different temperatures with the soft robotic gripper: a peach of ambient temperature ( $\approx 24$  °C), a peach of relatively low temperature ( $\approx 17$  °C), and a peach of relatively high temperature ( $\approx 36$  °C).

during object manipulation. We demonstrate the thermosensation and mechanosensation capabilities of this robotic gripper when performing “pick–hold–place” operations of peaches with different temperatures, as shown in Figure 5c. We used peaches of ambient temperature ( $\approx 24$  °C), relatively low temperature ( $\approx 17$  °C), and relatively high temperature ( $\approx 36$  °C) as the objects of demonstration. It is observed that when the robotic gripper grasps, holds, and releases the peach of ambient temperature, the thermal sensor signal keeps relatively stable without significant variation (Figure 5d). In contrast, when the robotic gripper grasps the cold peach or the warm peach, the thermal sensor signals exhibit an obvious decline or upswing respectively (Figure 5e,f). As the robotic gripper releases the cold peach or the warm peach, the sensor signal outputs recover gradually. These results verify the thermosensation functionality of this soft robotic gripper. During the “pick–hold–place” operations, the mechanical sensor signals show reproducible “increase–maintain–decrease” patterns (Figure 5d,f), confirming the mechanosensation functionality of this soft robotic gripper. Remarkably, the signal outputs of the mechanical sensor exhibit nearly identical patterns despite the temperature difference of the peaches, revealing that temperature variation does not affect

the mechanosensation functionality. The presented integration of soft robotic gripper with the potentiometric thermosensation and mechanosensation devices opens up new opportunities for the achievement of safe, agile, and sophisticated object manipulations for future robots.

## 2.6. Potentiometric Electronic-Skin for Thermosensation and Mechanosensation

To closely mimic the thermosensation and mechanosensation functions of natural skin, we designed a potentiometric e-skin with  $3 \times 3$  thermal sensors and  $4 \times 4$  mechanical sensors, as illustrated in Figure 6a left. The fabrication process of the e-skin is depicted in Figure S11, Supporting Information. Briefly, conductive gold connections are inkjet printed on a flexible substrate as the bottom electrode. PB/carbon sensing electrode patterns for both thermosensation and mechanosensation are stencil printed on the gold connections at the sensing regions. Then, the Ag/AgCl reference electrode pattern is printed by the side of the PB/carbon sensing electrodes with a gap of  $\approx 750$   $\mu\text{m}$ . Thermal sensors are fabricated by casting PVA/NaCl/Gly-2% ionic

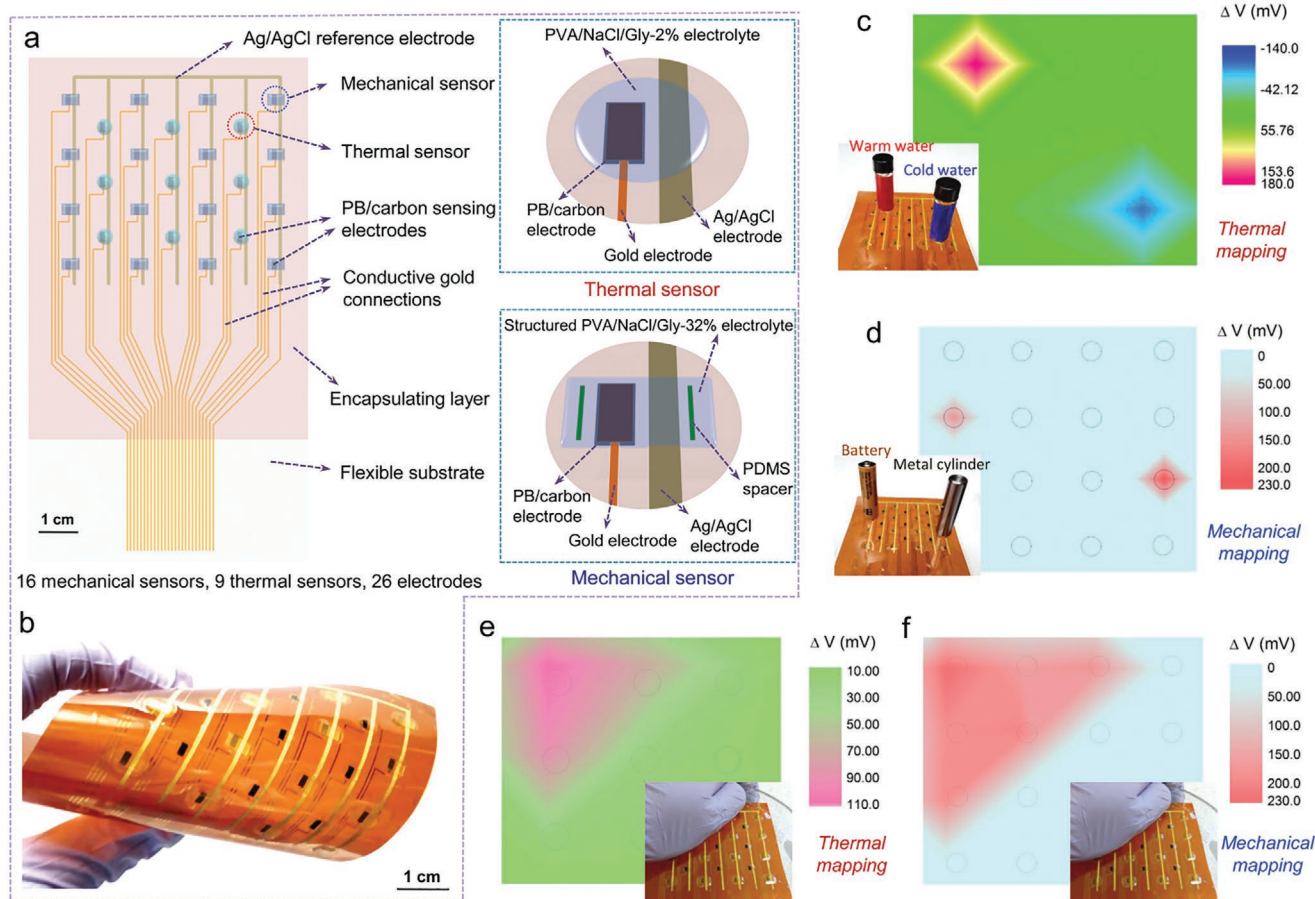


**Figure 6.** Potentiometric e-skin for both thermosensation and mechanosensation. a, b) Schematics illustrating the structural layout of a potentiometric e-skin integrated with  $3 \times 3$  thermal sensors and  $4 \times 4$  mechanical sensors (a) and photograph showing the final potentiometric e-skin (b). c) Signal outputs of the thermal sensors when a vial filled with  $\approx 65$  °C warm water (marked as red) and a vial filled with  $\approx 1$  °C cold water (marked as blue) are placed on the e-skin. d) Signal outputs of the mechanical sensors when a battery ( $\approx 23$  g) and a metal cylinder ( $\approx 43$  g) are placed on the e-skin. e, f) Spatial mappings in the signal outputs of the thermal sensors (e) and the mechanical sensors (f) when a warm hand is pressed onto the e-skin.

composite on the sensing regions, and mechanical sensors are constructed by placing microstructured PVA/NaCl/Gly-32% ionic composite on the sensing regions. The structural layouts of the thermal sensors and the mechanical sensors are illustrated in Figure 6a right. The resultant potentiometric e-skin, as shown in Figure 6b, features a single-electrode-mode configuration. Specifically, for an e-skin with  $N$  sensing pixels, only  $N + 1$  electrodes are needed as depicted in Figure S12a, Supporting Information. The basic principle is, for the potentiometric sensing mechanism, we are measuring the potential difference between two electrodes. Thus, we can use a single electrode as a reference point for the whole e-skin and measure the potential differences of other sensing pixels with respect to this reference point. This operation style can greatly simplify the fabrication and improve the pixel density of the e-skin when compared to conventional dual-electrode-mode e-skins (where  $2N$  electrodes are usually needed). More importantly, this potentiometric e-skin has self-generated signal outputs and does not rely on external power supply, featuring ultralow power consumption. The thermal and mechanical sensors in the e-skin also exhibit desirable device uniformity (Figure S12b,c, Supporting Information).

To evaluate the thermosensation behavior of the e-skin, glass vials filled with warm water of  $\approx 65$  °C and cold water of  $\approx 1$  °C are placed on the 1st–1st and 3rd–3rd pixels of the thermal sensor array (Figure 6c inset). The mapping in the signal outputs of the thermal sensors is reconstructed and given in Figure 6c. The 1st–1st sensing pixel under the warm object shows a significant increase in the measured potential difference output, while the 3rd–3rd sensing pixel beneath the cold object exhibits an obvious decrease in the measured signal output. The reconstructed color mapping is in good accordance with the distribution of the applied thermal stimuli. To evaluate the mechanosensation behavior of the e-skin, a battery of  $\approx 23$  g and a metal cylinder of  $\approx 43$  g are put on to the 2nd–1st and 3rd–4th pixels of the mechanical sensor array (Figure 6d inset). From the reconstructed color mapping (Figure 6d), it is noticed that the heavier object gives rise to a higher potential difference output of the corresponding sensing pixel, and the pressure mapping is also consistent with the object distribution. Moreover, this potentiometric e-skin is qualified with simultaneous thermosensation and mechanosensation functionalities. As a demonstration, a warm hand is pressed onto the e-skin (Figure 6e,f). Based on the mapping in the thermal sensor outputs (Figure 6e), the temperature variation is mainly located around the top left corner of the e-skin and the highest temperature is measured at the 1st–1st sensing pixel (corresponding to the central part of the palm). From the mapping in the mechanical sensor outputs (Figure 6f), the pressure applied by the palm is mainly distributed at the top left corner of the e-skin, which agrees with the actual situation. These results verify the good capability of this potentiometric e-skin for both thermosensation and mechanosensation in an energy-efficient way.

### 3. Conclusion

In summary, we have demonstrated a new type of potentiometric e-skin for simultaneous thermosensation and mechanosensation. Through component and structural manipulation

of the electrolyte carefully, thermal stimulus and mechanical stimulus can be detected simultaneously based on thermally regulated intrinsic impedance variation of the electrolyte and mechanically regulated electrode/electrolyte interfacial impedance variation. The proposed potentiometric thermosensation or mechanosensation principle allows us to monitor both static and dynamic thermal or mechanical stimuli without an external power supply, compensating for the deficiencies of the existing passive sensing devices in these regards. Leveraging this potentiometric sensing scheme, a soft robotic gripper and a passive e-skin for both thermosensation and mechanosensation are demonstrated. The presented e-skin features a single-electrode-mode configuration, all-solution-processing fabrication, simplified operation, ultralow power consumption, ultrahigh sensitivity, and good capability for simultaneous temperature mapping and pressure mapping. We envision that this innovative potentiometric e-skin can find promising applications in the emerging fields of skin prosthetics, humanoid robotics, wearable healthcare devices, bioelectronics, and other smart systems.

### 4. Experimental Section

*Fabrication of Potentiometric Thermal Sensors:* PB/carbon and Ag/AgCl electrodes with a side-by-side configuration were prepared via stencil printing method. Kapton tape films ( $\approx 60$   $\mu\text{m}$  in thickness) were laser-cut into defined patterns as the stencil and attached to a flexible PET substrate (125  $\mu\text{m}$  in thickness). PB/carbon ink (C2070424P2, Gwent Electronic Materials Ltd.) was first stencil-printed on the PET substrate using a polished glass slide, followed by drying the ink at 100 °C for 10 min. Then, Ag/AgCl ink (Cl-4001, Engineered Materials Systems, Inc.) was stencil printed on the substrate as another electrode. The two electrodes were then cured at 130 °C for 1 h. After peeling off the Kapton film stencil, PB/carbon sensing electrode and Ag/AgCl reference electrode with defined patterns were fabricated. The surfaces of the PB/carbon electrode and Ag/AgCl electrode were cleaned with flexible wiping papers (TechniCloth, Texwipe Company) dipped with ethanol to remove the additives from the inks left on the surface, thus to obtain clear and stable electrodes.

For the fabrication of the thermal sensors,  $\approx 25$  mg PVA/NaCl/Gly aqueous solutions containing 25 wt% PVA, 100 mM NaCl, and a certain amount of Gly (the weight ratios of Gly to PVA vary from 0.5% to 4.0%) were dropped on the sensing area of the side-by-side electrodes. Then, the PVA/NaCl/Gly solutions on the electrodes were first dried in a fume hood at ambient temperature for 2 weeks, followed by further drying and stabilizing in an environmental chamber at 25 °C and 50% RH for 2 days. Subsequently, the whole devices were encapsulated with Kapton tape films ( $\approx 60$   $\mu\text{m}$  thick) to minimize the effect of external environment on the sensing behavior of the thermal sensors.

*Preparation of Potentiometric Mechanical Sensors:* PB/carbon and Ag/AgCl electrodes were prepared as mentioned above. The microstructured PVA/NaCl/Gly ionic composites were prepared based on a solution casting method. Specifically, PVA/NaCl/Gly aqueous solutions containing 25 wt% PVA, 100 mM NaCl, and a certain amount of Gly (weight ratios of Gly to PVA vary from 16% to 64%) were cast onto a template with a periodic microstructure molded from a screen mesh (Figure S6, Supporting Information). The cast PVA/NaCl/Gly solutions were first dried in a fume hood at ambient temperature for 2 weeks, followed by further drying and stabilizing in an environmental chamber at 25 °C and 50% RH for 2 days. After drying, the microstructured PVA/NaCl/Gly ionic composite films ( $\approx 700$   $\mu\text{m}$  in thickness) were peeled off from the template and cut into defined shape and size. To fabricate the mechanical sensors, two PDMS spacers ( $\approx 0.18$  mm  $\times$  0.6 mm  $\times$  4 mm) were set near the two electrodes at the sensing area, followed by placing

a piece of PVA/NaCl/Gly ionic composites at the sensing area. The PDMS spacers were used to separate the PVA/NaCl/Gly electrolyte and the two electrodes, thus to normalize the initial signal output of the sensors into zero when no external stimulus was applied on the device. Subsequently, the whole devices were encapsulated with a layer of Kapton tape film ( $\approx 60 \mu\text{m}$  in thickness). To enhance the sensitivity of the mechanical sensors, force collectors ( $\approx 0.24 \text{ mm} \times 2.3 \text{ mm} \times 2.3 \text{ mm}$ , made of laser-cut Kapton tape films) were fixed on the top of the sensors at the sensing area, which could effectively transfer the externally applied force into the deformation of the microstructured electrolyte.

**Fabrication of Potentiometric Electronic-Skin:** The fabrication of the potentiometric e-skin with  $4 \times 4$  mechanical sensors and  $3 \times 3$  thermal sensors is depicted in Figure S11, Supporting Information. First, gold nanoparticle ink (Harima gold nanopaste ink model: NPG-J) was inkjet-printed on a Kapton tape film ( $\approx 60 \mu\text{m}$ , Bertech) using a Dimatix DMP 2800 inkjet printer with  $30 \mu\text{m}$  drop spacing and  $10 \text{ pL}$  drops. The inkjet-printed gold electrode pattern was first predried on the printer hotplate at  $60 \text{ }^\circ\text{C}$  for 30 min to stabilize the electrode pattern, followed by transferring the gold electrode pattern to a vacuum hotplate and annealing the gold electrode at  $250 \text{ }^\circ\text{C}$  for 1 h to fuse the gold nanoparticles into continuous conductive pattern. Then, a Kapton tape film ( $\approx 60 \mu\text{m}$  thick) was laser-cut into defined patterns as the stencil for stencil printing of PB/carbon and Ag/AgCl electrodes. The stencil was aligned with the gold electrode pattern carefully. Subsequently, PB/carbon and Ag/AgCl electrode patterns were stencil printed onto the gold electrode based on the conditions as mentioned above. After curing the PB/carbon and Ag/AgCl electrodes, the final e-skin electrode patterns were prepared. The thermal sensors were prepared using PVA/NaCl/Gly-2% ionic composite as the electrolyte, and the mechanical sensors were fabricated using microstructured PVA/NaCl/Gly-32% ionic composite ( $\approx 400 \mu\text{m}$  in thickness) as the electrolyte. The drying and stabilizing processes of the electrolyte, along with the assembly process of the mechanical sensors, are mentioned above. Finally, the thermal and mechanical sensor arrays were fully encapsulated with a layer of Kapton tape films ( $\approx 60 \mu\text{m}$  thick), resulting in the resultant potentiometric e-skin.

**Characterization and Measurement:** The voltage signal outputs of the thermal sensors, the mechanical sensors, and the e-skin were collected on a Keithley 2601A source meter using a voltage measurement mode (sourcing nearly zero current and measuring the voltage output). It is worth pointing out that the sensor outputs measured with different equipment could be different, because different measurement setups had different internal impedances. It was necessary to keep the measurement equipment constant to obtain consistent sensing behaviors. The force measurement was conducted on a lab-built setup based on a computer controlled movable stage and a digital force gauge (M5, Mark-10). Temperature calibration was conducted in a water bath with controlled temperature. Optical microscopic observation of the microstructured PVA/NaCl/Gly ionic composites was conducted on a Nikon optical microscope (Eclipse 50i). A Dektak profiler (Veeco 6M) was used for the profile measurement of the microstructured ionic composites. During the potentiometric mechanosensation process, some interferential spike signals might appear occasionally due to the triboelectric effect, which could be easily filtered via signal processing.<sup>[27]</sup>

## Supporting Information

Supporting Information is available from the Wiley Online Library or from the author.

## Acknowledgements

The authors acknowledge Jasmine Jan for helpful discussions. This work was supported in part by the Bakar Fellows Program, the National Science Foundation under Grant No. 1610899 and FlexTech Alliance under Grant No. AFOSR 42299.

## Conflict of Interest

X.W. and A.C.A. are inventors on a patent application (Provisional No. 62/939523) filed through the University of California, Berkeley. The other authors declare that they have no competing interests.

## Data Availability Statement

The data that support the findings of this study are available from the corresponding author upon reasonable request.

## Keywords

electronic skins, mechanical sensors, potentiometric sensing, robotics, thermal sensors

Received: December 16, 2020

Revised: January 11, 2021

Published online: February 22, 2021

- [1] A. Chortos, J. Liu, Z. Bao, *Nat. Mater.* **2016**, *15*, 937.
- [2] H. Hensel, *Annu. Rev. Physiol.* **1974**, *36*, 233.
- [3] M. Campero, H. Bostock, *Neurosci. Lett.* **2010**, *470*, 188.
- [4] V. E. Abaira, D. D. Ginty, *Neuron* **2013**, *79*, 618.
- [5] R. S. Johansson, J. R. Flanagan, *Nat. Rev. Neurosci.* **2009**, *10*, 345.
- [6] L. E. Osborn, A. Dragomir, J. L. Betthausen, C. L. Hunt, H. H. Nguyen, R. R. Kaliki, N. V. Thakor, *Sci. Rob.* **2018**, *3*, eaat3818.
- [7] Q. Li, L.-N. Zhang, X.-M. Tao, X. Ding, *Adv. Healthcare Mater.* **2017**, *6*, 1601371.
- [8] R. D. Giacomo, L. Bonanomi, V. Costanza, B. Maresca, C. Daraio, *Sci. Rob.* **2017**, *2*, eaai9251.
- [9] R. A. Kishore, S. Priya, *Materials* **2018**, *11*, 1433.
- [10] M. L. Hammock, A. Chortos, B. C.-K. Tee, J. B.-H. Tok, Z. Bao, *Adv. Mater.* **2013**, *25*, 5997.
- [11] Y. Wu, Y. Liu, Y. Zhou, Q. Man, C. Hu, W. Asghar, F. Li, Z. Yu, J. Shang, G. Liu, M. Liao, R.-W. Li, *Sci. Rob.* **2018**, *3*, eaat0429.
- [12] Y. Zang, F. Zhang, C. Di, D. Zhu, *Mater. Horiz.* **2015**, *2*, 140.
- [13] T. Someya, Y. Kato, T. Sekitani, S. Iba, Y. Noguchi, Y. Murase, H. Kawaguchi, T. Sakurai, *Proc. Natl. Acad. Sci. U. S. A.* **2005**, *102*, 12321.
- [14] N. T. Tien, S. Jeon, D.-I. Kim, T. Q. Trung, M. Jang, B.-U. Hwang, K.-E. Byun, J. Bae, E. Lee, J. B.-H. Tok, Z. Bao, N.-E. Lee, J.-J. Park, *Adv. Mater.* **2014**, *26*, 796.
- [15] J. Shin, Z. Liu, W. Bai, Y. Liu, Y. Yan, Y. Xue, I. Kandela, M. Pezhoouh, M. R. MacEwan, Y. Huang, W. Z. Ray, W. Zhou, J. A. Rogers, *Sci. Adv.* **2019**, *5*, eaaw1899.
- [16] F. Zhang, Y. Zang, D. Huang, C. Di, D. Zhu, *Nat. Commun.* **2015**, *6*, 8356.
- [17] J. Park, M. Kim, Y. Lee, H. S. Lee, H. Ko, *Sci. Adv.* **2015**, *1*, e1500661.
- [18] D. H. Ho, Q. Sun, S. Y. Kim, J. T. Han, D. H. Kim, J. H. Cho, *Adv. Mater.* **2016**, *28*, 2601.
- [19] Q. Hua, J. Sun, H. Liu, R. Bao, R. Yu, J. Zhai, C. Pan, Z. L. Wang, *Nat. Commun.* **2018**, *9*, 244.
- [20] C. Hou, H. Wang, Q. Zhang, Y. Li, M. Zhu, *Adv. Mater.* **2014**, *26*, 5018.
- [21] G. Y. Bae, J. T. Han, G. Lee, S. Lee, S. W. Kim, S. Park, J. Kwon, S. Jung, K. Cho, *Adv. Mater.* **2018**, *30*, 1803388.
- [22] B. Shih, D. Shah, J. Li, T. G. Thuruthel, Y.-L. Park, F. Iida, Z. Bao, R. Kramer-Bottiglio, M. T. Tolley, *Sci. Rob.* **2020**, *5*, eaaz9239.
- [23] K.-Y. Chun, Y. J. Son, E.-S. Jeon, S. Lee, C.-S. Han, *Adv. Mater.* **2018**, *30*, 1706299.
- [24] R. Ikeda, M. Cha, J. Ling, Z. Jia, D. Coyle, J. G. Gu, *Cell* **2014**, *157*, 664.

- [25] M. L. Jin, S. Park, Y. Lee, J. H. Lee, J. Chung, J. S. Kim, J.-S. Kim, S. Y. Kim, E. Jee, D. W. Kim, J. W. Chung, S. G. Lee, D. Choi, H.-T. Jung, D. H. Kim, *Adv. Mater.* **2017**, *29*, 1605973.
- [26] H.-H. Chou, A. Nguyen, A. Chortos, J. W. F. To, C. Lu, J. Mei, T. Kurosawa, W.-G. Bae, J. B.-H. Tok, Z. Bao, *Nat. Commun.* **2015**, *6*, 8011.
- [27] X. Wu, M. Ahmed, Y. Khan, M. E. Payne, J. Zhu, C. Lu, J. W. Evans, A. C. Arias, *Sci. Adv.* **2020**, *6*, eaba1062.
- [28] J. Owen, *Comprehensive Polymer Science and Supplements*, (Eds: G. Allen, J. C. Bevington), Pergamon, Oxford, UK **1996**, p. 669.
- [29] V. d. Z. Bermudez, M. M. Silva, *Polymer Electrolytes Fundamentals and Applications* (Eds: C. Sequeira, D. Santos), Woodhead, Cambridge, UK **2010**, p. 176.
- [30] S. Kuyucak, S.-H. Chung, *Biophys. Chem.* **1994**, *52*, 15.
- [31] K. M. Diederichsen, H. G. Buss, B. D. McCloskey, *Macromolecules* **2017**, *50*, 3831.
- [32] X. Tang, X. Wang, R. Cattley, F. Gu, A. D. Ball, *Sensors* **2018**, *18*, 4113.
- [33] G. Sebald, D. Guyomar, A. Agbossou, *Smart Mater. Struct.* **2009**, *18*, 125006.
- [34] D. Zabek, F. Morini, *Therm. Sci. Eng. Prog.* **2019**, *9*, 235.
- [35] J. Park, Y. Lee, M. Ha, S. Cho, H. Ko, *J. Mater. Chem. B* **2016**, *4*, 2999.
- [36] S. Sundaram, P. Kellnhofer, Y. Li, J.-Y. Zhu, A. Torralba, W. Matusik, *Nature* **2019**, *569*, 698.